On-Chip Bimetallic Plasmo-Thermomechanical Detectors for Mid-Infrared Radiation

Qiancheng Zhao, Parinaz Sadri-Moshkenani, Mohammad Wahiduzzaman Khan, Rasul Torun, and Ozdal Boyraz

***Abstract*— We present an on-chip radiation detector based on the bimetallic plasmo-thermomechanical fishbone nanowire arrays that are suspended on a silicon nitride waveguide to provide modulation on the propagating mode in the waveguide due to thermomechanical deflection. The design concept is scalable from visible to infrared (IR) spectrum. To demonstrate the concept, we design the suspended fishbone nanowires that are 18.6 μm long. The nanowire is composed of six strip antenna unit cells, and each unit cell has an absorption coefficient of 42.4% at 4.3-μm target wavelength. The nanowire array includes nine wires with a period of 3.1 μm. The device has a figure of merit of 2.64 × 10^{-2} $\mu m^2/\mu W$. We investigate the modulation strength with respect to the IR radiation density at 4.3 μm, and the optimum readout power in the waveguide to avoid self-heating is also discussed.**

***Index Terms*— Infrared detectors, bimetallic nanobeam, plasmonic antennas, thermoplasmonics, thermomechanics.**

I. Introduction

THE fundamental concept behind the infrared (IR) detection is the transduction mechanism that enables the energy conversion from the electromagnetic domain to the others. Depending on the energy transduction mechanism, most of the infrared detectors can be classified as either quantum or thermal detectors [1]. The thermoplasmonics, which takes advantage of the photo-thermal effect induced by resonant light absorption in metallic nanostructures, has become an appealing direction in nanoscale heat sources [2]. Heat transformed by the thermal generators induces temperature change, and can be measured by the temperature-dependent mechanisms, which include pyroelectricity [3], thermoelectricity [4], conductivity [4], thermo-optics [6], [7], mechanical deflections [8], [9], etc. Among these mechanical thermal detectors, bimaterial devices play an important role. The bimaterial thermal detectors usually utilize the cantilevers or the suspended membranes that deflect due to thermal expansion. To convert the tiny mechanical deflection into a measurable quantity, optical systems are often employed based on trigonometry [10]–[12] or interferometry [13], [14]. However, these optical systems require discrete bulky lenses and detectors, hence they are difficult to miniaturize. Inspired by the metal-based evanescent field modulators [15] and our recent achievement of the optical leaky wave antennas (OLWAs) [16], here we propose a novel on-chip plasmo-thermomechanical detector for IR radiation detection. To be specific, the free space target IR radiation is absorbed by the fishbone nanowires and creates thermo-mechanical deflection on the suspended wires. The gap between the nanowires and the underneath waveguide is selected to have an evanescent field interaction that causes attenuation on the waveguided mode. Thus, the change in the target IR radiation intensity is read out by the attenuation on the transmitted power in the waveguides at the probe wavelengths, which can be easily realized by an on-chip photo detector. The proposed design embraces the capability for on-chip integration and the flexibility for operation due to the separation of the target and probe wavelengths. In particular, we show the optimized design for the target wavelength at 4.3 μm and probe wavelength at 1550 nm. The fishbone nanowire array consists of 9 suspended fishbone nanowires that are 18.6 μm long. The nanowire has 6 strip antenna unit cells. To assess the performance of the device, the figure of merit (FOM) is defined as the ratio of the change in S_{21} in the waveguide with respect to the illumination power density, namely $\Delta|S_{21}|/I_{IR}$, where I_{IR} is the IR power density in the unit of W/m^2. The figure of merits (FOMs) of the proposed device is 2.64 × 10^{-2} $\mu m^2/\mu W$.

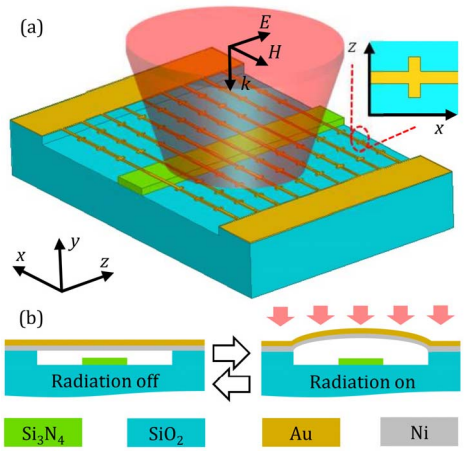

Fig. 1. Schematic geometry (a) and operation principle (b) of the bilayer plasmo-thermomechanical detector for IR radiation. The inset in (a) shows the top view of the antenna unit cell.

II. Device Model, Simulation Results and Discussion

As demonstrated in Fig. 1(a), the operation of the detector needs the interplay of three key elements: strip antennas,

Manuscript received March 16, 2017; revised June 6, 2017; accepted July 14, 2017. Date of publication March 16, 2017; date of current version August 2, 2017. This work was supported by the National Science Foundation under NSF Award ECCS-1449397. *(Corresponding author: Qiancheng Zhao.)*

The authors are with the Department of Electrical Engineering and Computer Science, University of California at Irvine, Irvine, CA 92697 USA (e-mail: qianchez@uci.edu; psadrimo@uci.edu; mohammwk@uci.edu; rtorun@uci.edu; oboyraz@uci.edu).

Color versions of one or more of the figures in this letter are available online at http://ieeexplore.ieee.org.

Digital Object Identifier 10.1109/LPT.2017.2728373

bimetallic fishbone nanowires, and a waveguide. When the infrared energy is absorbed by the resonant metal strips, the absorbed energy is conducted to the nanowires and creates a thermal gradient. The temperature variation will thermally actuate the nanowires, changing the gap between the nanowires and the waveguide top surface, as illustrated in Fig. 1(b). In our design, the deformation of the nanowires modulates the evanescent field from the waveguide whose dimension is 1.5 μm $\times$ 0.3 μm to guarantee the single TE mode at 1550 nm wavelength. The gap between the nanowires and the waveguide determines the strength of the interaction, which is set to be 50 nm, a separation that has enough evanescent field interaction, and that is also fabrication feasible, e.g., etching the silicon dioxide (SiO_2) sacrifice layer with hydrogen fluoride (HF) acid vapor. For the sake of fabrication compatibility, gold (Au) and nickel (Ni) are used to build the nanowires due to their chemical resistance to HF. Since Au has a larger thermal expansion coefficient (14.2 $\times$ 10^{-6}/K) than Ni (13.4 $\times$ 10^{-6}/K), Au should be placed on top of Ni, so that the nanowire will bend upward to avoid collapsing and sticking to the waveguide surface. The amount of deflection of nanowires is determined by the relative thickness of each layer, the temperature gradient, and the length of the nanowire. Below we show how to optimize the nanowires for maximum deflection and hence optical modulation on the propagating waves.

The detection system is modeled and simulated in three parts, being the plasmo-thermal conversion, the thermo-mechanical deflection, and the evanescent field modulation. We use the finite element method based software (COMSOL Multiphysics) to solve all three parts. The composition of the nanowire is first settled by the thermo-mechanical simulation. The temperature-induced bending of the double clamped bilayer beam (inset in Fig. 2) is a function of the thermal expansion coefficient γ, layer thickness t, and temperature profile $T(x)$ as described in Eq. (1) and (2) [17], [18]:

$$\frac{d^2\Delta y}{dx^2} = 6\left(\gamma_2-\gamma_1\right)\frac{t_1+t_2}{t_2^2 K}\left[T\left(x\right)-T_0\right] \tag{1}$$

$$K = 4+6\left(\frac{t_1}{t_2}\right)+4\left(\frac{t_1}{t_2}\right)^2+\frac{E_1}{E_2}\left(\frac{t_1}{t_2}\right)^3\frac{1-\nu_2}{1-\nu_1} + \frac{E_2}{E_1}\left(\frac{t_2}{t_1}\right)\frac{1-\nu_1}{1-\upsilon_2} \tag{2}$$

where $\Delta y(x)$ is the vertical deflection of the beam at the position x and the origin is located at the center of the beam, E is the Young's modulus, ν is the Poisson's ratio. The subscripts 1 and 2 represent the top and the bottom layers. The ambient temperature is denoted by T_0.

As formulated in Eq. (1), a thick wire may reduce the amount of deflection. However, if the wire is too thin, it may not have enough mechanical strength for suspension. Here, we set the wire thickness $t_1 + t_2$ to be 50 nm as a tradeoff between the mechanical strength and the amount of deflection of the wire. Given a temperature profile $T(x) - T_0 = \Delta T \cdot (1 - (2x/l)^2)$ where l is the length of the beam and ΔT is the temperature difference at the beam center, the amount of deflection is estimated to be

$$\Delta y\left(x\right) = 24\left(\gamma_2-\gamma_1\right)\frac{t_1+t_2}{t_2^2 K}\cdot\Delta T l^2 \times\left(-\frac{1}{2}\left(\frac{x}{l}\right)^4+\frac{1}{8}\left(\frac{x}{l}\right)^2-\frac{5}{192}\right) \tag{3}$$

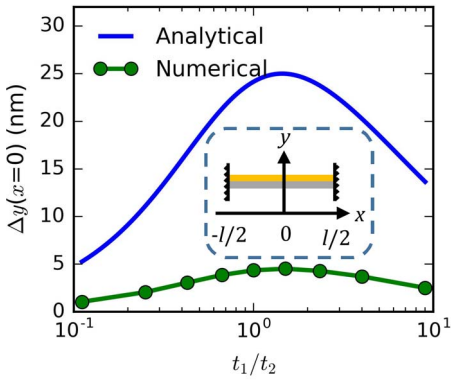

Fig. 2. Comparison of the displacement in the center of the beam as a function of the top and bottom layer thickness ratio, t1/t2, using the analytical formula and the FEM simulation method. The inset shows the schematic of the double clamped bilayer beam.

Figure 2 illustrates the analytical and numerical estimation of the deformation for the Au and the Ni composed layers. In these calculations, we assume a beam length $l = 10$ μm, beam width W_b = 100nm (for numerical analysis only), and $\Delta T = 100$ K. The shortcoming of the analytical method arises from the fact that it does not consider the wire width in calculations, hence the analytical result is 5 times higher than the rigorous numerical analysis. This mismatch has also been explained in [12] and reported in the support information of [13]. Despite the discrepancy of the peak values, the analytical and numerical solutions agree well that the ratio of the Au and Ni layer thickness should be 1.5.

In our design, strip antennas are employed to absorb the infrared radiation and to generate thermal gradient. To increase the total absorbed energy, multiple antennas are connected by a single nanobeam, yielding a fishbone-like nanowire. The strip antenna, surrounded by air and suspended 350 nm above the SiO_2 substrate, is optimized in a unit cell (inset in Fig. 3(b)) in terms of the strip length L_s, strip width W_s, and periods in the x and z directions. The beam width W_b is set to be 100 nm in our study. As shown in Fig. 3(a), increasing the width of the strip will reduce the resonant length and lower the absorption coefficient. We find out that the combination of $L_s = 1.77$ μm and W_s = 100 nm yields the highest absorption coefficient at $\lambda = 4.3$ μm. The periods in the x and z directions are optimized simultaneously to achieve $P_x = P_z$. The absorption coefficient reaches a peak value of 0.424 when the periods equal 3.1 μm in both x and z directions as shown in Fig. 3(b).

For demonstration purpose, we design a fishbone nanowire that includes 6 strip antenna unit cells. The total length of the wire, $l = 18.6$ μm, is selected as a compromise of fabrication challenges and the amount of deflection of the wire. The two ends of the nanowire are connected to the metal pads which act as heat sinks, and the temperature of the two ends are then set to be 293.15 K. The heat transfer coefficient on the wire surface is assigned to be 5 W/(m^2 $\cdot$ K) to mimic

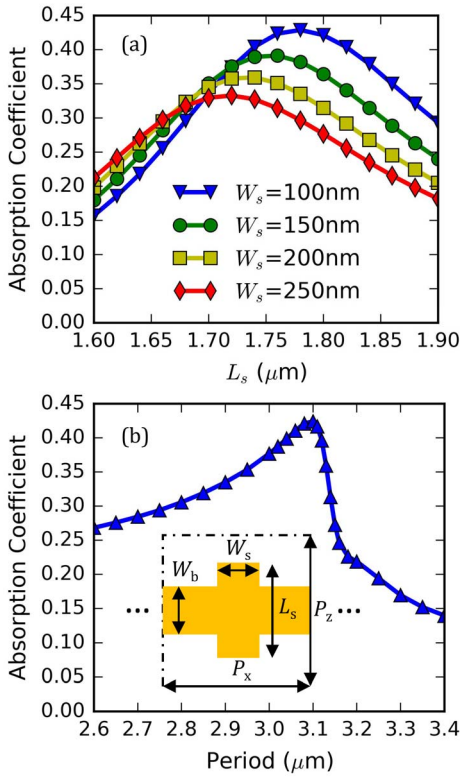

Fig. 3. The absorption coefficients as functions (a) of the strip length L_s and strip width W_s for a given period of $P_x = P_z = 3.1$ μm, and (b) of the period for a given strip with $L_s = 1.77$ μm and $W_s = 100$ nm. The inset in (b) shows the antenna unit cell in top view. The unit cells are connected in the x direction.

the stagnant air cooling condition. For a 4 μW/μm^2 normal incident power density (z-polarized) at 4.3 μm wavelength, the highest temperature on the nanowire can reach 428.16 K, and the temperature profile along the nanowire is quasi-parabolic as depicted in the inset of Fig. 4(a). Figure 4(a) also illustrates that the maximum temperature $T_{\max}$ on the nanowire increases linearly with respect to the incident power density. The slope of the curves indicates that the temperature-IR power density conversion ratio η_{TI} is 33.75 K/(μW/μm^2) for this device.

The thermal expansion caused by the temperature increment will deflect the nanowire upwards due to difference in the thermal expansion coefficients of Au and Ni. Since the Si_3N_4 waveguide is located at the center of the nanowire, only the displacement at the beam center is studied here. By feeding the temperature profile generated by the 4 μW/μm^2 radiation power density into the thermomechanical model, the maximum deflection at the center of the nanowire is found to be 23.5 nm as shown in Fig. 4(b). Since the temperature profile is quasi-parabolic, the displacement-temperature conversion ratio, η_{DT}, can be approximated from Eq. (3):

$$\eta_{\mathrm{DT}} = \frac{\partial \Delta y\,(0)}{\partial \Delta T} = -\frac{5}{8}\,(\gamma_2 - \gamma_1)\,\frac{t_1 + t_2}{t_2^2 K} l^2 \cdot \zeta \qquad (4)$$

where l is 18.6 μm for the current device, and ζ is the fitting parameter to match the numerical and simulation results and it is equal to 0.197, and the corresponding η_{DT} is 0.17 nm/K, meaning that a 1 K temperature increment in the beam center will elevate the nanobeam center by 0.17 nm.

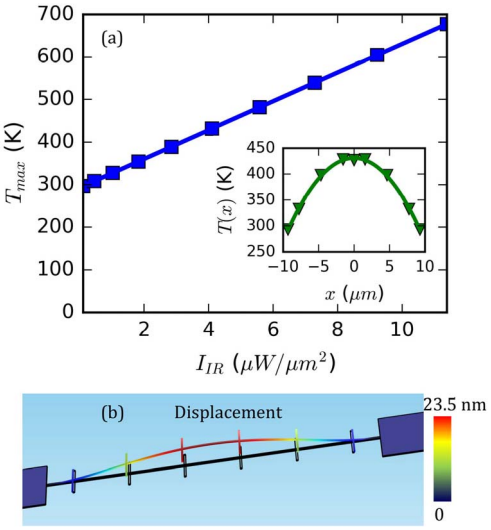

Fig. 4. (a) The maximum temperature of the nanowire as a function of the IR power density. The inset shows the temperature profile along the nanowire when the input power density is 4 μW/μm^2. (b) The displacement profile of an 18.6 μm long fishbone nanowire under 4 ìW/îm2 irradiation power density. The shadow shows the original position of the wire.

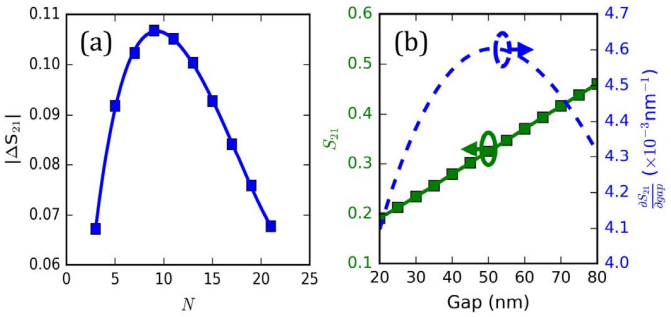

Fig. 5. (a) The differences of the S_{21} parameters, ΔS_{21}, at gap = 50 nm and gap = 73.5 nm are plotted as a function of the number of nanowires N. (b) S_{21} parameter as a function of the gap is shown as the green curve on the left axis. The derivative of S_{21} with respect to the gap is plotted as the dashed blue curve on the right axis.

The fishbone nanowires are periodically arranged along the waveguide direction (the z direction), to form an OLWA and modulate the propagating wave in the waveguide. Instead of measuring the radiation patterns like we did for OLWAs [16], the change of the waveguide output power, $\Delta P_{\mathrm{wg,out}}$, at the radiation *on* and *off* states is of interest here, because it is a measurable quantity by an on-chip photo detector. For fair comparison, we normalize the variation of the waveguide output power to its input power, yielding the change of the S_{21} parameter, ΔS_{21}. The number of the nanowires, N, affects ΔS_{21} in a way that too few wires limit the modulation strength, while too many wires can attenuate the output power severely, making it challenging to measure ΔS_{21}. Assuming that the gap changes from 50 nm to 73.5 nm in the IR radiation *off* and *on* states, a sweep of N finds that ΔS_{21} reaches the maximum when N equals 9, and the peak value is 0.106, as shown in Fig. 5(a), indicating a modulation depth of 10% on the transmitted power in the waveguide.

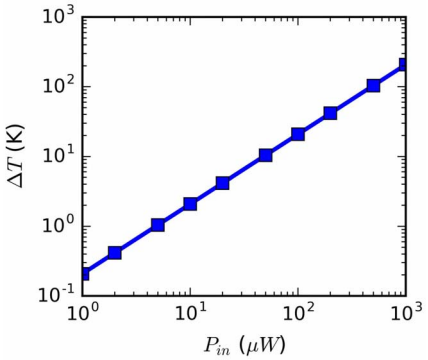

Fig. 6. The maximum temperature difference ΔT' at the center of the nanowire as a function of the waveguide input power P_{in}. The gap between the nanowire and the waveguide top surface is 50 nm.

With the chosen wire number $N = 9$, the S_{21} as a function of the change of the gap is studied to reveal the sensitivity of S_{21} to the gap variation, η_{SD}, as shown in Fig. 5(b). When the gap is 50 nm, 1 nm increment in the gap will result in 4.6×10^{-3} shift in S_{21} parameter.

Combining all the conversion ratios from the electromagnetic domain to the thermal domain and then to the mechanical domain and finally back to the optical domain, the figure of merit (FOM) of the device is defined as

$$\text{FOM} = \frac{\partial S_{21}}{\partial I_{\text{IR}}} = \eta_{\text{SD}}\eta_{\text{DT}}\eta_{\text{TI}} \tag{5}$$

For the proposed device, its FOM is 2.64×10^{-2} $\mu\text{m}^2/\mu\text{W}$, indicating that 1 $\mu\text{W}/\mu\text{m}^2$ radiation will result in 2.64×10^{-2} change in the waveguide S_{21} parameter.

It is worth noting that increasing the waveguide input power can enlarge the output power difference, but it will also heat the nanowire by its own evanescent field, leading to a larger gap than the designed value and desensitizing the detector. Since the waveguide is narrow compared to the nanowire, the waveguide can be viewed as a point heat source, and the temperature profile along the nanowire changes linearly with respect to positions, following $T(x) - T_0 = \Delta T' \cdot (1 - 2|x|/l)$, where $\Delta T'$ is the center temperature difference caused by the waveguide heating. With the linear temperature distribution, η'_{DT} becomes

$$\eta'_{DT} = \frac{\partial \Delta y\,(0)}{\partial \Delta T'} = -\frac{1}{2}\,(\gamma_2 - \gamma_1)\,\frac{t_1 + t_2}{t_2^2 K} l^2 \cdot \zeta' \tag{6}$$

where ζ' is the fitting parameter to match the numerical and theoretical results under the linear temperature distribution, and ζ' equals 0.233 in this study. The corresponding η'_{DT} is 0.16 nm/K. $\Delta T'$ as a function of the waveguide input power P_{in} is depicted in Fig. 6. When the input power is smaller than 100 μW, $\Delta T'$ will be less than 21 K, causing at most 3.36 nm self-heating deflection, which is an acceptable value.

III. Conclusion

In summary, we propose an on-chip bimetallic plasmo thermomechanical mid-IR detector that uses waveguided modes to detect IR incident wave through the evanescent field modulation. The design is scalable and can be applied to wavelengths from mid-IR to near-IR, i.e., detecting 785 nm [19]. FOM is used to characterize the device performance, but it can also be converted to the responsivity in the unit of V/W. We estimate our device performance to be ~450.7 V/W, comparable to the work in [13] given the same system parameters, but with an advantage of 1/10 smaller probe light power and on-chip integration capability. This letter reports the proof-of-the-concept device not targeting to compete with the state-of-the-art semiconductor photo detectors. Detailed theoretical and experimental studies on the optimum sensitivity and bandwidth should be provided in future. Although we focus on the readout from the guided modes in this letter, it is also possible to detect the readout through the free space radiation by the leaky waves.

References

[1] A. Rogalski, "Infrared detectors: Status and trends," *Prog. Quant. Electron.*, vol. 27, nos. 2–3, pp. 59–210, 2003.
[2] N. J. Hogan, A. S. Urban, C. Ayala-Orozco, A. Pimpinelli, P. Nordlander, and N. J. Halas, "Nanoparticles heat through light localization," *Nano Lett.*, vol. 14, no. 8, pp. 4640–4645, Aug. 2014.
[3] G. Sebald, E. Lefeuvre, and D. Guyomar, "Pyroelectric energy conversion: Optimization principles," *IEEE Trans. Ultrason., Ferroelect., Freq. Control*, vol. 55, no. 3, pp. 538–551, Mar. 2008.
[4] J. P. Carmo, L. M. Goncalves, and J. H. Correia, "Thermoelectric microconverter for energy harvesting systems," *IEEE Trans. Ind. Electron.*, vol. 57, no. 3, pp. 861–867, Mar. 2010.
[5] J. B. Herzog, M. W. Knight, and D. Natelson, "Thermoplasmonics: Quantifying plasmonic heating in single nanowires," *Nano Lett.*, vol. 14, no. 2, pp. 499–503, Feb. 2014.
[6] M. R. Watts, M. J. Shaw, and G. N. Nielson, "Optical resonators: Microphotonic thermal imaging," *Nature Photon.*, vol. 1, no. 11, pp. 632–634, Nov. 2007.
[7] J. Zhu, S. Ozdemir, and L. Yang, "Infrared light detection using a whispering-gallery-mode optical microcavity," *Appl. Phys. Lett.*, vol. 104, no. 17, p. 171114, Apr. 2014.
[8] F. Zhang *et al.*, "Infrared detection based on localized modification of *Morpho* butterfly wings," *Adv. Mater.*, vol. 27, no. 6, pp. 1077–1082, Feb. 2015.
[9] H. Zhu, F. Yi, and E. Cubukcu, "Plasmonic metamaterial absorber for broadband manipulation of mechanical resonances," *Nature Photon.*, vol. 10, no. 11, pp. 709–714, Nov. 2016.
[10] J. R. Barnes *et al.*, "A femtojoule calorimeter using micromechanical sensors," *Rev. Sci. Instrum.*, vol. 65, no. 12, pp. 3793–3798, Dec. 1994.
[11] J. Lai, T. Perazzo, Z. Shi, and A. Majumdar, "Optimization and performance of high-resolution micro-optomechanical thermal sensors," *Sens. Actuators A, Phys.*, vol. 58, no. 2, pp. 113–119, Feb. 1997.
[12] R. Lefevre *et al.*, "Numerical study of bimetallic actuated micromembrane with large deformations," *J. Micromech. Microeng.*, vol. 23, no. 1, p. 015011, 2013.
[13] F. Yi, H. Zhu, J. C. Reed, and E. Cubukcu, "Plasmonically enhanced thermomechanical detection of infrared radiation," *Nano Lett.*, vol. 13, no. 4, pp. 1638–1643, Apr. 2013.
[14] J. A. Batlle and G. A. Berini, "Nonlinear micro/nano-optomechanical oscillators for energy transduction from IR sources," Ph.D. dissertation, Dept. Eng. Electron., Univ. Autònoma Barcelona, Bellaterra, Spain, 2015.
[15] G. A. Magel, "Integrated optic devices using micromachined metal membranes," *Proc. SPIE*, vol. 2686, pp. 54–63, Mar. 1996.
[16] Q. Zhao, C. Guclu, Y. Huang, F. Capolino, and O. Boyraz, "Experimental demonstration of directive Si_3N_4 optical leaky wave antennas with semiconductor perturbations," *J. Lightw. Technol.*, vol. 34, no. 21, pp. 4864–4871, Nov. 1, 2016.
[17] R. J. Roark and W. C. Young, *Formulas for Stress and Strain*, 5th ed. New York, NY, USA: McGraw-Hill, 1975.
[18] M. Manna, F. Magistrali, M. Maini, and D. Reichenbach, "Finite element method applied to stress simulation of high power 980 nm pump lasers," *Microelectron. Rel.*, vol. 37, nos. 10–11, pp. 1667–1670, Oct. 1997.
[19] Q. Zhao, P. Sadri-Moshkenani, M. W. Khan, R. Torun, I.-U. Zaman, and O. Boyraz, "Infrared detection using plasmonically enhanced thermomechanically actuated nanowire arrays," in *Proc. Conf. Lasers Electro-Opt.*, 2017, paper JTh2A.114.